Modeling the Effects of the Factors Affecting IGF in Coastal Areas and Variation of IGF in Jiaodong Peninsula of China Based on Finite Element Method

Hong-Xu Chu
Shandong University at Weihai
Zan-Yang Xing (xingzanyang@sdu.edu.cn)
Shandong Medical Institute: Shandong University https://orcid.org/0000-0001-5965-1017
Yan-Ling Wang
Shandong University at Weihai
Balan Nanan
Shandong University at Weihai
Qing-He Zhang
Shandong University
Li-Kai Liang
Shandong University at Weihai
Han Wang
Shandong University at Weihai

Research Article

Keywords:

Posted Date: January 27th, 2022

DOI: https://doi.org/10.21203/rs.3.rs-1096104/v2

Abstract

Based on finite element method, we develop a model of the induced geoelectric field (IGF) occurring in land-sea boundary regions during large geomagnetic field disturbances. The model is used first to study the effects of the changes in the lithospheric conductivity, ionospheric current, and ocean depth on the distribution of IGF in a typical land-sea boundary region. The results show that the changes in the lithospheric conductivity and ionospheric current (frequency, magnitude and direction) have major effects and ocean depth has minor effect on IGF in coastal areas. Then by incorporating a realistic 3-D conductivity variation of Jiaodong Peninsula (JDP) in China obtained from measured data, the model is used to simulate the IGF variation in JDP covering its land-sea boundaries for east-west and north-south ionospheric currents. The results show a new aspect that extremely large IGF development on the land side of the coastal bay areas perpendicular to the currnet compared to plane coastal areas. The results can stimulate detailed investigations of IGF (and GIC, geomagnetically induced current) in coastal areas.

Key Points

- Finite element method is used to model the effects on IGF of the changes in coastal conductivity, ionospheric current and ocean depth.
- The changes in the conductivity and ionospheric current and frequency are found to be the major factors affecting IGF in coastal areas.
- The IGF modeled using the observed conductivity values in coastal bay areas are over twice as strong as in plane areas.

Plain Language Summary

During space weather, the high-energy solar wind with frozen-in magnetic field interact with the Earth's magnetosphere-ionosphere system, causing violent fluctuations in the geomagnetic field and induced geoelectric field (IGF) and geomagnetically induced current (GIC) in ground-based

systems especially in coastline areas. IGF and GIC increase the reactive power loss of power transmission systems and even cause transformer failure. It has therefore been important to investigate the effects on IGF of the changes in coastal conductivity, ionospheric current frequency and strength, and ocean depth in sea-land boundaries. In this paper, using a newly developed conductivity model we first investigate the effects of these changes on IGF in a typical sea-land boundary and then study the IGF variation in the coastal area of Jiaodong Peninsula in China using observed conductivities. The results show a new aspect that IGF in bay boundaries are over twice as strong as in plane boundaries.

1 Introduction

Large geomagnetic disturbances caused by solar storms such as ICMEs (interplanetary coronal mass ejections) are known to produce induced geoelectric field (IGF) in the earth, ocean and other conducting

media. IGF causes geomagnetically induced current (GIC) flow in the electrical loop formed by the utility systems such as electric power grids, telecommunication networks, etc. and the earth. The systems get damaged when GIC exceeds their tolerance limit (Wang, 2003; Kappaenman, 1996, 2003;Wang et al., 2021)[1-3].

GIC is generally strong at high latitudes due to the strong geomagnetic field there undergoing large and violent changes during space weather events. Many GIC related utility system damages happened in the high latitude regions such as Northern Europe and North America during severe space weather events. For example, the event on 13 March 1989 damaged the Quebec power transformer causing power outage for over five million people for over nine hours (Kappaenman & Albertson, 1990; Pulkkinen et al., 2005). In recent years, China, Australia, New Zealand, Japan and other countries in middle and low latitudes have also experienced GIC infringements in power grids (Cui et al., 2010; Wu & Liu., 2013; Liu et al., 2016; Marshall et al., 2013; Clilverd et al., 2020; Shigeru et al., 2018). Studies also found that coastal areas are more prone to GIC impacts than inland areas. For example, in December 2006, significant levels of GIC were detected in the Guangdong Lingao and Jiangsu Shanghe substations in China. Comparative studies during the event showed that the GIC level in the lower latitude substation (Guangdong Lingao) was larger than that in the higher latitude substation (Jiangsu Shanghe) (Liu et al., 2009) due to the "coast effect". That is, the electrical conductivity in coastal areas (Guangdong Lingao) are stronger and more complex than in inland areas (Jiangsu Shanghe) (Fernberg et al., 2007).

Though the main cause of IGF is solar storms such as ICMEs, the distribution of IGF in the earth depends on the electrical properties of the earth. Studying the influence of the electrical structure of the earth on the distribution of IGF is therefore the key to assess the GIC level in power grids, which have been undertaken by many scientific groups. In the earlier calculations of IGF distribution, scientists have used the plane wave method (Viljanen et al., 2006) and complex image method (Pulkkinen et al., 2007). These methods considered the earth as a horizontally layered one-dimensional structure and ignored the lateral changes of earth’s conductivity. The methods therefore are not suitable for calculating the IGF distribution in coastal areas having large lateral conductivity changes.

Recently, scientists have used two-dimensional earth conductivity models to calculate the IGF generated in coastal areas. It is found that IGF has increased greatly in the land area up to about 50km away from the sea-land interface. This has been explained in terms of the coastal effect, that is, the distribution of IGF is greatly affected by the lateral change of the earth's conductivity (Olsen & Kuvshinov, 2004; Gilbert, 2005). Liu et al. (2016; 2017) developed an one-dimensional (1-D) and three-dimensional (3-D) geodetic conductivity models for the local area along the coast of Guangdong Lingao, and calculated the IGF during the super the geomagnetic storm on November 9, 2004. The accuracy of the GIC value calculated by the 3D model of IGF is 18% higher than that by the 1D model. But there is still a gap of 12% compared with the measured data (Liu et al., 2016; 2017). The reason for the difference between the 3D model and data may be due to the insufficient fitting of the Earth’s electrical structure.

In this article, we use an effective numerical calculation method - the finite element method - to develop a 3D earth conductivity model in the sea-land boundary region and calculate the geomagnetic field and IGF. The finite element method has a very wide range of applications in successfully reflecting the structural relationship of complex materials and calculations in the field of electromagnetic fields. It has better performance than other numerical calculation methods in dealing with complex free boundary conditions. Since the complex geodetic conductivity model involves the connections of many boundaries of different conductivity regions, the free boundary conditions are very complicated. The finite element method can well solve the problem of handling these free boundary conditions. The 3D model is used first to study the effects of lithospheric conductivity, ionospheric current (frequency, magnitude and direction), and ocean depth on the distribution of IGF in a typical land-sea boundary region. Then the 3D model is extended to construct a conductivity model for the land-sea boundary area of the Jiaodong Peninsula (JDP) in China by using the measured data of the geological environment of Jiaodong Peninsula (JDP). The 3D model is uded to simulate the distribution of IGF in JDP under east-west and north-south currents.

2 Mathematical Model Of Igf

As mentioned above, we use the finite element method to develop a mathematical model of the induced geoelectric field (IGF). Two assumptions (Honkonen et al., 2018) are used in the model. (1) Rotation and curvature of the earth are ignored and modeling and analysis are performed in Cartesian coordinate system. (2) The magnetic permeability in all solution domains is assumed to be the vacuum magnetic permeability μ_0 (= $4\pi \times 10^{-7}$H/m). The assumptions are valid for calculating IGF especially in local areas such as JDP.

Figure 1 illustrates the IGF mathematical model. The whole solution domain Ω is divided into the conductor area Ω_1, non-conductor area Ω_2, and interface Γ. The conductor area Ω_1 is composed of the conductive earth, sea water and other geological structures. The non- conductor area Ω_2 is composed of air and ionospheric current source J_s. The interface Γ between Ω_1 and Ω_2 is the surface of the earth shown by the horizontal line. e_n is a unit vector normal to the interface Γ directed from Ω_1 to Ω_2. Based on the physical properties of the electromagnetic field, properties of the medium and boundary constraints, the finite element method is used first to mesh the solution domain, that is, divide the domain into sub-units. Then, refine the mesh at the interface where the electrical conductivity changes greatly, and coarsen the mesh at the areas where the electrical conductivity is uniform.

In order to simplify the calculation of the three-dimensional geoelectric field, the vector magnetic potential $\vec{A}$ and scalar magnetic potential ϕ are used as the functions to be calculated at each node of the sub-unit. The geomagnetic field $\vec{B}$ and the geoelectric field $\vec{E}$ are expressed as:

$$\vec{B} = \nabla \times \vec{A}$$

1
\stackrel{`}{E}=-(\frac{?\stackrel{`}{A}}{?t}+?f)
2

The basic equation of the three-dimensional IGF mathematical model is (Ma, 2016):

\frac{1}{{\mu }_{0}}\nabla \times \nabla \times \overrightarrow{A}+\sigma \left(\frac{\partial \overrightarrow{A}}{\partial t}+\nabla \phi \right)=\overrightarrow{{J}_{s}}
3
\nabla \bullet \sigma \bullet \left(\frac{\partial \overrightarrow{A}}{\partial t}+\nabla \phi \right)=0
4

where {\sigma } is the conductivity of the conductive medium.

The interface conditions of different conductivity regions are:

{e}_{n}\times \left(\frac{1}{{\mu }_{0}}\nabla \times \overrightarrow{{A}_{2}}-\frac{1}{{\mu }_{0}}\nabla \times \overrightarrow{{A}_{1}}\right)=0
5
\overrightarrow{{A}_{2}}=\overrightarrow{{A}_{1}}
6
{\phi }_{2}={\phi }_{1}
7
{e}_{n}\bullet {\sigma }_{2}\left(\frac{\partial \overrightarrow{{A}_{2}}}{\partial t}+\nabla {\phi }_{2}\right)={e}_{n}\bullet {\sigma }_{1}\left(\frac{\partial \overrightarrow{{A}_{1}}}{\partial t}+\nabla {\phi }_{1}\right)
8

{\sigma }_{1} and {\sigma }_{2} are the conductivities, {A}_{1} and {A}_{2} are the vector magnetic potentials, and {\phi }_{1} and {\phi }_{2} are the scalar magnetic potentials of the land and sea, respectively.

The boundary of the earth conductor area satisfies the first boundary condition:

\overrightarrow{{A}_{2}}=\overrightarrow{{A}_{0}}
9

The boundary of the air area satisfies the second boundary condition:

{e}_{n}\times \left(\frac{1}{{\mu }_{0}}\nabla \times \overrightarrow{{A}_{2}}\right)=\overrightarrow{{K}_{0}}
10

Equation 10 specifies the tangent component of the geomagnetic field as the boundary condition and applies in the form of surface current density \overrightarrow{{K}_{0}}. The ground serves as the interface

between the earth conductor and the air area (Figure 1). According to current continuity at the interface, there is

{e}_{n}\bullet \sigma \times \left(\frac{\partial \overrightarrow{A}}{\partial t}+\nabla \phi \right)=0
11

Equations (3) to (11) are the basic equations and boundary conditions of the 3-D geoelectric field boundary value problem in time domain. When the specific forms of the current source J_s in Ω_2 and the conductivity distribution in Ω_1 are given, the \overrightarrow{A} and {\phi } of each node of any sub-unit in the field can be obtained. Then when all the sub-units are combined, the \overrightarrow{B} and \overrightarrow{E} in the solution domain are obtained from formulas (1) and (2). We use the AC/DC module in the COMSOL AB Multiphysics®v.5.4. software developed at Stockholm in Sweden and available at cn.comsol.com to calculate and simulate the ground conductivity and IGF distribution.

3 Model Setup

In the modeling procedure, the conductivity of land and seabed is set to a typical value of 0.01 S/m up to 100km below the surface since both land and seabed belong to the lithosphere. Taking into account the skin effect of the electromagnetic field, the skin depth is calculated for a surface current of frequency of 0.003 Hz and current density 100 A/m^2 in the ground with a conductivity of 0.01 S/m. The calculation results show that the electromagnetic field at a depth of 400km is ~1% of the surface electromagnetic field. Therefore, the lower boundary of the model is set at a depth of 400km. In order to avoid the influence of the lateral boundary conditions on the IGF, the left and right boundaries are set at 500km from the center. At the lateral tion boundaries, the electromagnetic wave is complteley absorbed though theoretically the boundary can extend to infinity.

The ocean depth is set at 4 km considering the average global ocean depth of 3688 m, and the ocean conductivity is set at 4 S/m, the average conductivity of sea water. Since geomagnetic disturbances arise mainly from the changes in the storm-time ionospheric current, these disturbances are simulated by assuming the current. Following Pulkkinen et al. (2007), the current is considered as a thin uniform current sheet at a height of 100 km above the earth's surface. Assuming that the ionospheric current frequency is 0.003 Hz, the surface current density is set at 100 A/m^2. The surface current in the model starts from the boundary on one side to the boundary on the corresponding side, which is a continuous current that runs through the entire model. The ionospheric current generates magnetic waves propagating down to the earth and induces the geoelectric field. To simulate the attenuation effect of air on the waves, the atmospheric conductivity is set at 1.8×10^{-4} S/m in the region between the ionospheric current and earth surface. The upper boundary of the model is set 50km above the sheet current, and electromagnetic waves are completely absorbed at the boundary. Figure 2(a) shows the ground conductivity model of the land-sea boundary area. Figures 2(b) and 2(c) display the calculated underground (X-Z plane with Y=0) magnetic field and IGF, and Figures 2(d) and 2(e) display the calculated surface (X-Y plane with Z=0) magnetic field and IGF, respectively.

As shown by Figures 2b and 2d, the magnetic field in the ocean area is concentrated on the ocean surface (reddish-yellow strip in Figure 2b) and does not extend much below the surface; the magnetic field in the land area, though weak at the surface, extends well below the surface. The IGF (Figures 2c and 2e) is concentrated within a small distance on the land side of the land-sea interface, with amplitude up to 115 mV/km at the center of the interface; beyond the small distance, IGF gradually decreases to nearly uniform value laterally. In the sea side there is almost no IGF. The main point in Figure 2 is the illustration of the 'coastal effect'. That is, IGF gets concentrated within a small area on the land side of the land-sea interface. The coastal effect therefore should be considered seriously in GIC risk assessment.

Comparing (a) and (b), it can be found that the distribution of IGF in the two figures is basically the same without considering the size and frequency of the sheet current. It shows that using this model to analyze the distribution of IGF is effective.

3.1 Effects of different factors on IGF

As mentioned in section 1, IGF is affected by many factors such as conductivity, ionospheric current (frequency, magnitude and direction), ocean depth, etc. The effects of these factors on IGF are investigated in this section.

3.1.1 Effect of conductivity

The conductivity of slate in common sedimentary rocks and metamorphic rocks are found to be in ~0.001-0.1 S/m range and quartzite in magmatic rocks and metamorphic rocks are in ~0.0001-0.01 S/m range. To cover these ranges, in the model (Figure 2a), we use the lithospheric conductivity in ~0.0001-0.1 S/m range. Other conditions are same as in the model. As shown in Figures 4-5, when the conductivity increases from 0.0001 to 0.1 S/m, in the land side the maximum IGF (IGFmax) at the center of the land-sea interface decreases from 368.3 mV/km to 24 mV/km. For all conductivity values, IGF decreases rapidly within a short distance and stabilizes gradually at a long distance from the interface (Figure 5). The stars indicate the distances (~20-30 km) where IGF becomes 50% of IGFmax and dots indicate the distances (~150-90 km) where IGF nearly stabilizes when conductivity increases from 0.0001 to 0.01 S/m. In the sea side, IGF suddenly decreases to a value of zero for all conductivities.

The fact that IGFmax decreases from high to low values (368 mV/km to 24 mV/km) with the increase of lithospheric conductivity (0.0001 to 0.01 S/m) indicates that the conductivity is a major factor influencing the IGF in coastal areas. The greater the difference in electrical conductivity between land and ocean, the greater the magnitude of IGF generated in the land-sea boundary area, and the more severe the impact of the coastal effect.

3.1.2 Effects of ionospheric current

The ionospheric current during geomagnetic storms can affect IGF through changes in frequency, magnitude and direction. The effects of these aspects are studied here. The storm-time ionospheric

current is found to have periodic variations with periods ~100-1000s (Xu, 2000). We use current of frequency 0.001-0.01 Hz; all other conditions remain the same as in the model (Figure 2a).

The simulation results (Figures 6-7) show that IGFmax decreases rapidly from 153 mV/km to 52 mV/km when the current frequency increases from 0.001 Hz to 0.01 Hz. The decrease of IGF with distance from the interface (Figure 7) is similar to that for the conductivity (Figure 5) though IGFmax for the current case is only about half. Stars and dots indicate the distance where IGF becomes 50% of IGFmax (~25-65 km) and nearly stabilizes (~125-60 km), respectively, for frequency 0.001-0.006 Hz. Like conductivity, the ionospheric current frequency is a major factor influencing the strength IGF in coastal areas.

The effect of ionospheric current density on IGF is shown in Figure 8; (a), (b) and (c) are surface IGF for current density 50 A/m^2, 100 A/m^2 and 200 A/m^2 with all other conditions same as in the model (Figure 2a). As shown, magnitude of IGFmax at the interface is nearly equal to that of current density indicting that the severity of IGF (and GIC) depends directly on the severity of storm-time ionospheric current. To study the effect of ionospheric current direction, the current (100 A/m^2) is changed to be parallel to the land-sea interface; all other conditions are same as for Figure 8b. In this case (Figure 8d), there is no IGF at the interface and IGF in inland areas is slightly decreased compared to when the current is perpendicular to the interface (Figure 8b). The results (Figure 8) indicate that IGF (and GIC) are strong in coastal areas where the current is perpendicular to the sea-land interface.

3.1.3 Effect of ocean depth

The ocean is generally considered to have two parts, the sea and ocean. The ocean is the main body which has a depth of ~3-100 km and sea is the shallow ocean-land boundary having depth up to 3 km. The coastal area includes the coastal land area and the adjacent sea-ocean boundary area. Considering that there is rarely any deep ocean in the sea-land boundary area, the ocean depth is set to vary from 1 to 3 km. All other conditions remain the same as in the model (Figure 2a). There is only a small change in IGF (Figure 9) when ocean depth increases from 1 to 3 km.

The corresponding IGFmax at the interface is found to decrease by a small amount from 139.2 mV/km to 100 mV/km. With distance from the interface, the IGF rapidly decreases and becomes nearly constant at ~50 km away from the interface for all ocean depths (line curves not shown). The results indicate that the ocean depth has only a minor effect on IGF.

4 Modeling The Igf In Jiaodong Peninsula

Jiaodong Peninsula (JDP, Figure 10a) is located in the north-eastern coastal area of China at (34.4°-38.4°N, 114.3°-122.7°E). In order to protect the power grids of JDP from getting damaged due to large GIC, it is necessary to analyze the distribution of IGF in JDP. As discussed in section 3, lithospheric conductivity has strong impacts on IGF distribution in coastal areas. We obtain a realistic conductivity model in JDP covering its land-sea boundaries and simulate the distribution of IGF in JDP.

The electrical conductivity distribution map of JDP (Figure 10a) is obtained from China's deep geological section data set surveyed by the Institute of Geology (China Earthquake Administrator) and the China Environmental Geology zoning map drawn by the Institute of Hydrogeology and Environmental Geology (IHEG) of the Chinese Academy of Geological Sciences. The inset Table in Figure 10a lists the electrical conductivity distribution at different depths obtained for zones 1, 2 and 3. By using the listed conductivity distribution (Figure 10a), we simulate the distribution of IGF in JDP for both east-west and north-south ionospheric currents. The other parameters used are same as those in model Figure 2a (ionospheric current density 100 A/m^2 and current frequency 0.003Hz) which seem to correspond to large geomagnetic disturbances.

Figures (10b-c) show the simulated ground magnetic field and IGF in JDP for eastward currents and Figures (10d-e) show the same for northward currents, respectively. The east-west and north-south ionospheric currents have generated strong geomagnetic field in the sea-land boundary areas especially on the south and north sides and east side (Figure 10b-d), respectively; the field in eastern boundary area (Figure 10b) and inland area are significantly weak. IGF amplitude for east-west ionospheric current (Figure 10c) is larger on the southern side of the western land-sea boundary and a small part of the northern land-sea boundary. IGF on the south side is significantly greater (up to 540 mV/km) than that on the north side (up to 327 mV/km); and IGF at the land-sea boundary on the east side and most of the north side is small. Under the north-south ionospheric current (Figure 9e), large-amplitude IGF is generated at the land-sea boundary area on the north and south sides of the eastern part of JDP; IGF on the south side is significantly larger (up to 506 mV/km) than that on the north side (up to 175 mV/km). In particular, IGF is extremely large on bay sea-land boundaries than on non-bay boundaries. The maximum IGF in bay boundaries is up to 540 mV/km compared to the maximum IGF of 270 mV/km in non-bay boundaries. The areas of larger IGF amplitudes (or coastal effect) are within the range of a few tens of kilometers along the coast and IGF in inland areas are significantly small, discussed in section 5.

5 Discussion

As introduced in section 1, the variation of induced geoelectric field (IGF) in coastal areas have been studied earlier using different methods (Liu et al., 2009; Olsen & Kuvshinov, 2004; Gilbert, 2005). For example, Liu et al. (2009) and Liu and Wang (2016) used a plane wave model and finite element 3-D conductivity model, respectively, to calculate the IGF variation in Guangdong (China) during the extreme geomagnetic storm in 09 November 2004. The 3-D model was found to have 18% better agreement with the measured data than the 1-D model. Honkonen and Kuvshinov (2018) developed a global 3-D conductivity model and calculated the distribution of IGF on a global scale under the action of the equivalent ionospheric current source computed by Pulkkinen et al. (2007). The results have shown that the IGF in mid and high latitude coastal areas is much larger compared to low latitudes. The maximum IGF in high latitudes can reach 2.5 V/km and extends hundreds of kilometers inland.

In this paper we have developed a 3-D conductivity model based on the efficient finite element numerical calculation method (section 2). The model was used first (section 3) to show that the changes in

lithospheric conductivity and ionospheric current (frequency, magnitude and direction) and ocean depth have major and minor effects, respectively, on IGF in coastal areas at mid latitudes. In coastal areas, IGF develops on the land side with maximum at the interface (IGFmax) due to the accumulation of electric charge on the less conductive land side. With conductivity increasing from 0.0001 to 0.1 S/m (Figure 3 and Figure 4), IGFmax decreases from a high of ~385 mV/km to a low of 24 mV/km, and IGF rapidly decreases to ~50% of IGFmax at ~25-75 km and gradually stabilizes at a distances of ~130-25 km from the interface. Earlier, Santosh et al. (2018) reported IGF stabilizing at a short distance of 15 km from the interface; this seems to be due to the use of huge current (1 MA) and finite difference time domain method. With ionospheric current frequency increasing from 0.002 Hz to 0.01 Hz, IGFmax decreases from ~150 mV/km to 50 mV/km (Figure 5 and Figure 6). With ionospheric current, magnitude of IGFmax is nearly equal to that of the current density, and IGFmax becomes strongest when the current is perpendicular to the sea-land interface (Figure 8). Earlier, by using an ionospheric current of frequency 0.001Hz and density 1 A/m, Liu et al. (2017) obtained a much higher IGFmax of 2783 mV/km; they used land and ocean conductivities of 0.01 S/m and 4 S/m, respectively. With ocean depth, IGFmax decreases by a comparatively small amount (~140 to 100 mV/km) when the depth increases from 1 km to 5 km (Figure 9).

Then a realistic 3-D conductivity model of Jiaodong Peninsula (JDP) in China is constructed from measured data (Figure 10a), which is used to simulate the distribution of IGF in JDP under east-west and north-south ionospheric currents (section 4). The results (Figures 10b and 10e) indicate an important new aspect, that is, very strong coastal effect in bay areas. The maximum IGF in bay boundaries is up to 540 mV/km compared to the maximum IGF of 270 mV/km in non-bay boundaries. This is due to the electric charge accumulating all around the curved low conducting landside of the bay. The IGF on the south coastal area of JDP, especially in bay areas, is generally stronger than that on the north (Figures 10b and 10e). This may be because the topographic structure of the coastal area on the south side is more complicated than that on the north side. The sea-land boundary on the north side of the JDP is relatively smooth with no mountains and valleys, while the sea-land boundary on the south side is uneven. The electrical conductivity has multiple lateral abrupt changes in the uneven land-sea boundary, which has caused larger IGF in the coastal areas on the south side of the JDP compared to the north side. It is also found that the east-west and north-south ionospheric currents have different effects on the eastern and western coastal areas of JDP. This is because the sea-land boundary is perpendicular to the current. The land and sea boundaries in the western part of JDP are mostly north-south, and are greatly affected by the east-west ionospheric current. The eastern sea-land boundary is mostly east-west, and is greatly affected by the north-south ionospheric current.

6 Conclusions

By developing an earth electrical conductivity model based on finite element method we first modeled the effects of the factors affecting the induced geoelectric field (IGF) in a typical land-sea boundary region. The model has simulated the effects of the changes in lithospheric conductivity (0.0001-0.1S/m),

ionospheric current (frequency 0.001-0.01 Hz, density 50-200 A/m^2 and direction), and ocean depth (1-5 km) on IGF generation in a typical mid latitude coastal area. The results show that the conductivity, ionospheric current frequency and current density have major effects and ocean depth has minor effect on IGF; and perpendicular current has greater effect than parallel current. The IGF develops on the land side of the interface. The IGF decreases rapidly from IGFmax at the interface to 50% of IGFmax at ~25 km and then gradually decreases and stabilizes at ~125 km inland.

Then by using measured data, we constructed a realistic 3-D conductivity model of China's Jiaodong Peninsula (JDP) and simulated the IGF variation under east-west and north-south ionospheric currents. The results show that geomagnetic field disturbances have greater impacts on the coastal area on the south side of the JDP than on the north side. The east-west ionospheric current has greater impact on the western coastal areas and north-south ionospheric current has greater impact on the eastern coastal areas. An important new aspect is the development of extremely large IGF in coastal bay areas. The results can provide a theoretical basis for the GIC risk assessment of JGP and other coastal areas during severe space weather events.

Declarations

Acknowledgments

Thanks to the China Geological Survey Geological Cloud website for the China Geological Environment Zoning Map, Shandong Province Geological Environment Zoning Map and China Deep Geoscience Section Map Dataset. Thanks to the COMSOL Multiphysics software provided by COMSOL Inc. for modeling and simulation.

Authors' contributions

Hong-Xu Chu modeled the earth conductivity model, simulated the geomagnetic field and induced geoelectric field, and wrote the manuscript. Zan-Yang Xing guided the modeling process and revised the model. Balan Nanan explained the results and corrected the manuscript. Yan-Ling Wang, Qing-He Zhang, Li-Kai Liang, and Han Wang helped for the discussions. All authors read and approved the fnal manuscript.

Funding

The work was supported by the National Natural Science Foundation of China (Grants 41904169, 42120104003, 41604139, and 41874170), the Foundation of China Research Institute of Radiowave Propagation (Grant A132101W02), and the Chinese Meridian Project.

Availability of data and materials

The modeling data used in this article are available at https://doi.org/10.5281/zenodo.5543865.The model and simulation data are available on the website

of https://zenodo.org/record/5513720#.YUwfPeziubg.

Competing interests

The authors declare that they have no competing interests.

References

1. Wang J X. Explosive solar activity and disastrous sapce weather. Journal of Purple Mountain Observatory, 2003, (01), 49–58
2. Clilverd M.A., Rodger, C. J., Brundell, J. B., et al. (2020), Geomagnetically induced currents and harmonic distortion: High time resolution case studies. *Space Weather, 18*(10). doi:10.1029/2020SW002594
3. Cui, M. D.,Liu, C. M., Liu, L. G. (2010), Assessment of the Influence caused by solar storm on Sichuan power grid rated 500 kV. *High Voltage Technology, 36*(11), 2849–2855.
4. Fernberg, P. A., Samson, C., Boteler, D. H., et al. (2007), Earth conductivity structures and their effects on geomagnetic induction in pipelines. *Annales Geophysicae, 25*(11), 207–218. doi:10.5194/angeo-25-207-2007
5. Gilbert, J. L. (2005), Modeling the effect of the ocean-land interface on induced electric fields during geomagnetic storms. *Space Weather, 3*(4). doi:10.1029/2004SW000120
6. Honkonen, I., Kuvshinov, A., Rasttter, L., et al. (2018), Predicting global ground geoelectric field with coupled geospace and Three-Dimensional geomagnetic induction models. *Space Weather, 16*(8), 1028–1041. doi:10.1029/2018SW001859
7. Kappaenman, J. G. (1996), Geomagnetic storms and their impact on power systems. *IEEE Power Engineering Review, 16*(5). doi:10.1109/MPER.1996.491910
8. Kappaenman, J. G. (2003), Storm sudden commencement events and the associated geomagnetically induced current risks to ground-based systems at low-latitude and mid-latitude locations. *Space Weather, 1*(3). doi:10.1029/2003SW000009
9. Kappaenman, J. G., & Albertson, V. D. (1990), Bracing for the geomagnetic storms. *IEEE Spectrum, 27*(3), 27–33. doi:10.1109/6.48847
10. Liu, C. M., Lin, C. X., Wang, X. N., et al. (2017), Influence of coast effect on geomagnetic induced current in power grid. *Power System Technology, 41*(8), 2716–2722.
11. Liu, C. M., Wang, X., Liu, L. G., et al. (2016), Calculation method of geomagnetic induced current in Power Grid Considering coast effect. *Proceedings of the CSEE, 36*(22), 6059–6066.
12. Liu, L. G., Liu, C. M., Zhang, B. (2009), Effects of geomagnetic storm on UHV power grids in China. *Power System Technology, 33*(11), 1–5.
13. Liu, L. G., Yang, P. H., Guo, S. X., et al. (2016), Impact of Geoelectric Field Direction and AC System Structure on Geomagnetically Induced Currents in ±800 kV Mengxi Convertor Station. *Power System Technology, 40*(5), 1295–1300.

14. Ma, X, K. (2016), Electromagnetic field finite element and analytical combination method. *Beijing: Science Press*.
15. Marshall, R. A., Gorniak, H., Walt, T. V. D., et al. (2013), Observations of geomagnetically induced currents in the Australian power network. *Space Weather, 11*(1), 6–16. doi:10.1029/2012SW000849
16. Olsen, N., & Kuvshinov, A. (2004), Modeling the ocean effect of geomagnetic storms. *Earth Planets Space, 56*(5), 525–530. doi:10.1186/BF03352512
17. Pulkkinen, A., Hesse, M., Kuznetsova, M., Rastatter, L. (2007), First-principles modeling of geomagnetically induced electromagnetic fields and currents from upstream solar wind to the surface of the Earth. *Annales Geophysicae, 25*(4), 881–893. doi:10.5194/angeo-25-881-2007
18. Pulkkinen, A., Lindahl, S., Viljanen, A., et al. (2005), Geomagnetic storm of 29-31 October 2003: Geomagnetically induced currents and their relation to problems in the Swedish high-voltage power transmission system. *Space Weather, 3*(8). doi:10.1029/2004SW000123
19. Santosh, P., Bach, N., Miguel, R., et al. (2018), A Finite Difference Time Domain Investigation of Electric Field Enhancements Along Ocean-Continent Boundaries During Space Weather Events. *Journal of Geophysical Research: Space Physics, 123*(6), 5033–5046. doi:10.1029/2017JA024648
20. Shigeru, F., Ikuko, F., Arata, F., et al. (2018), Numerical modeling of spatial profiles of geomagnetically induced electric field intensity in and around Japan. *Technical Report of the Kakioka Magnetic Observatory, 14*(2), 35–50.
21. Viljanen, A., Pulkkinen, A., Pirjola, R., et al. (2006), Recordings of geomagnetically induced currents and a nowcasting service of the Finnish natural gas pipeline system. *Space Weather, 4*(10). doi:10.1029/2006SW000234
22. Wang, H., Xing, Z.-Y., Balan, N., Wang, Y.-L., Zhang, Q.-H., & Liang, L.-K. (2021). Simulation and analysis of geomagnetically induced current levels in Shandong Power Grid. Space Weather, 19, e2020SW002615. doi:10.1029/2020SW002615
23. Wang, J. X. (2003), Explosive solar activity and disastrous sapce weather. *Journal of Purple Mountain Observatory,* (01), 49–58.
24. Wu, W. L., & Liu, L. G. (2013), Analysis of the influence of magnetic storm disturbance on the voltage of long distance high voltage transmission system. *Science Technology and Engineeruing, 13*(16), 4579–4584+4590.
25. Xu, Y. S. (2000), Research Progress on electrical conductivity of mantle minerals and rocks. *Earth Science Frontiers, 7*(1), 229–237.

Figures

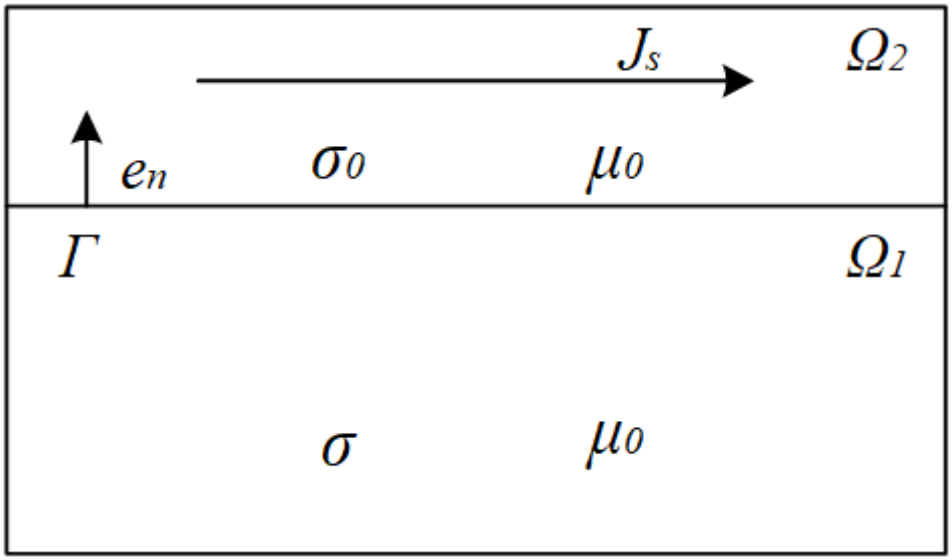

Figure 1

Mathematical model of induced geoelectric field (IGF).

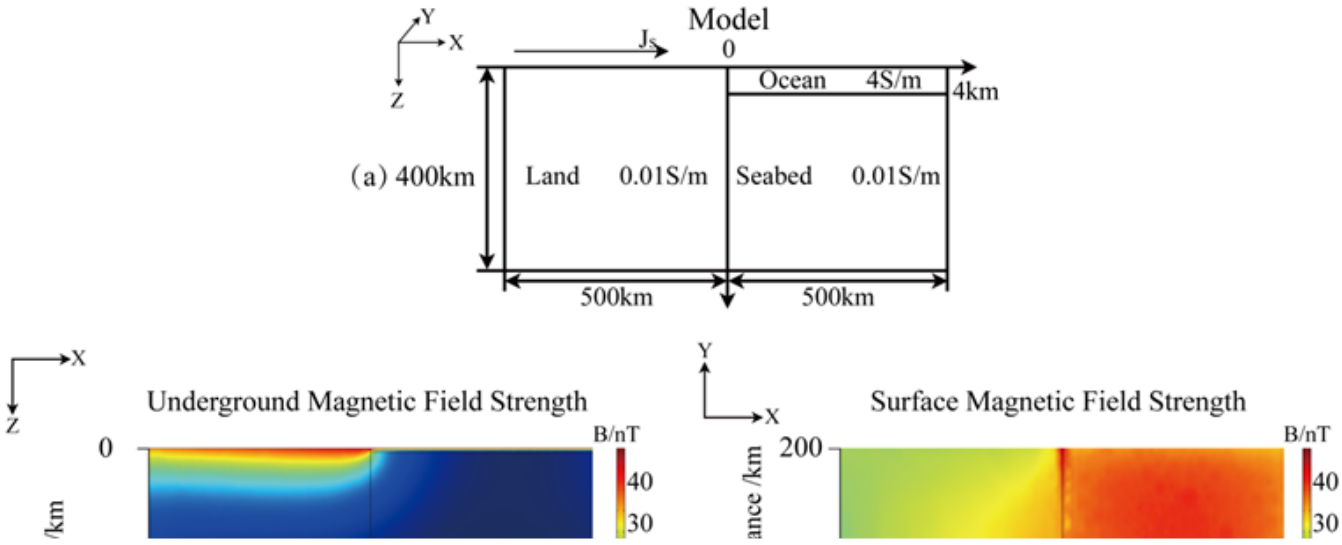

Figure 2

(a) Typical earth conductivity model of the land-sea boundary area, the ionospheric current Js is perpendicular to the sea-land boundary, the lithospheric conductivity is 0.01 S/m, the current density is 100 A/m^2, the current frequency is 0.003 Hz, and the ocean depth is 4 km. (b) and (c) display the underground magnetic field and IGF in X-Z plane (Y=0), and (d) and (e) display the surface magnetic field and IGF in the X-Y plane (Z=0).

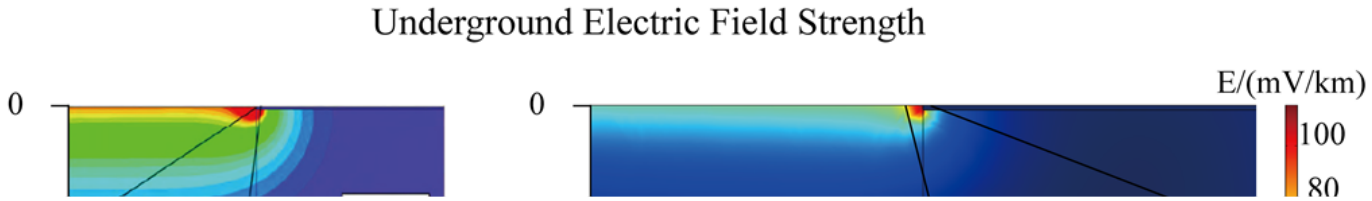

Figure 3

(a) The distribution of IGF calculated by Liu et al. (2017) under the conditions of earth conductivity 0.01S/m, sea water conductivity 4S/m, ocean depth 5km, sheet current 1A/m, and frequency 0.001Hz. (b) is the same as Figure 2 (c), and the interface area in both (a) and (b) are enlarged in the inset for clarity.

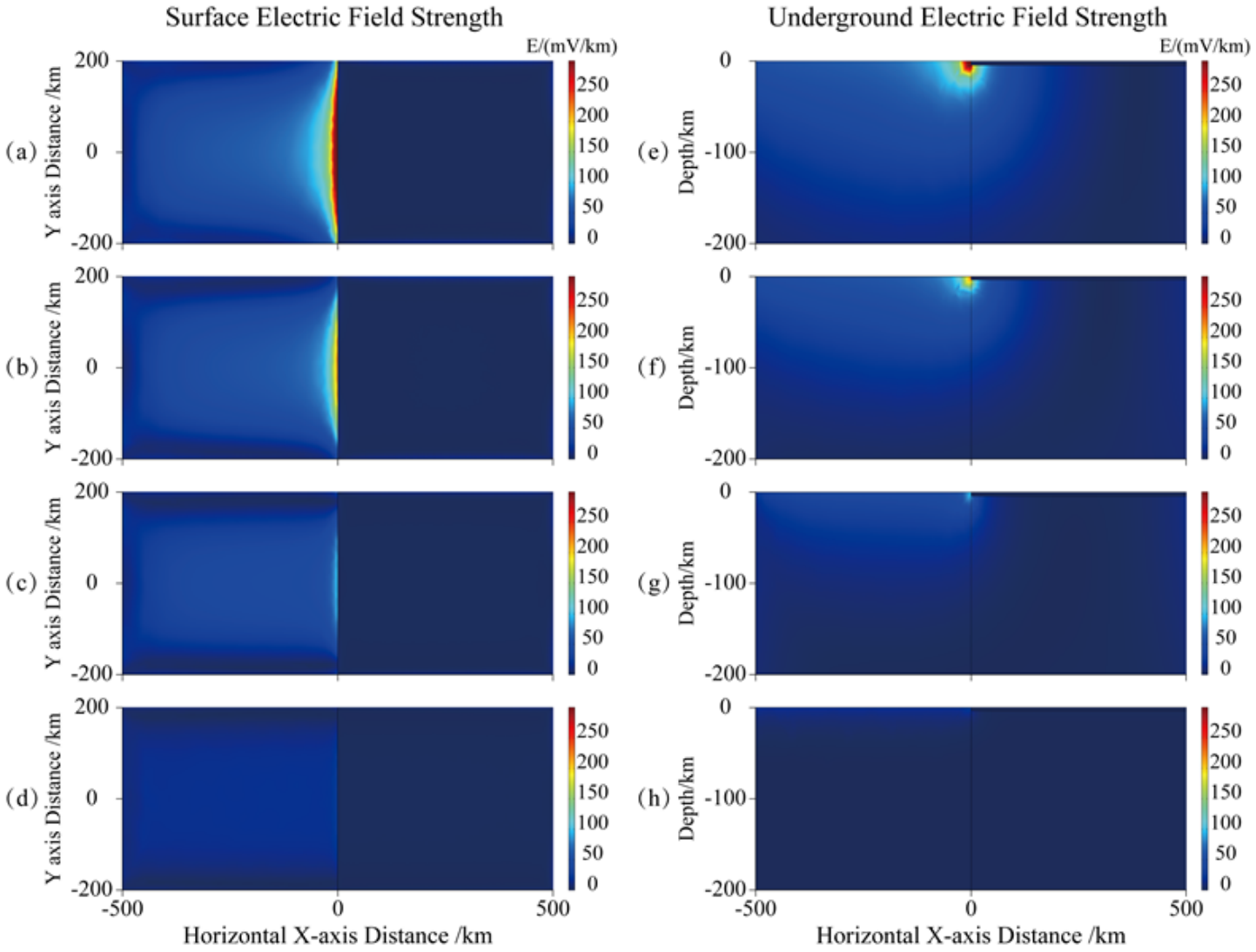

Figure 4

(a), (b), (c), (d) and (e), (f), (g), (h) show the distribution of surface IGF (X-Y plane with Z=0) and underground IGF (X-Z plane with Y=0), respectively, when the lithospheric conductivity is 0.0001, 0.001, 0.01 and 0.1 S/m (top to bottom). All other conditions are same as in the model (Figure 2a).

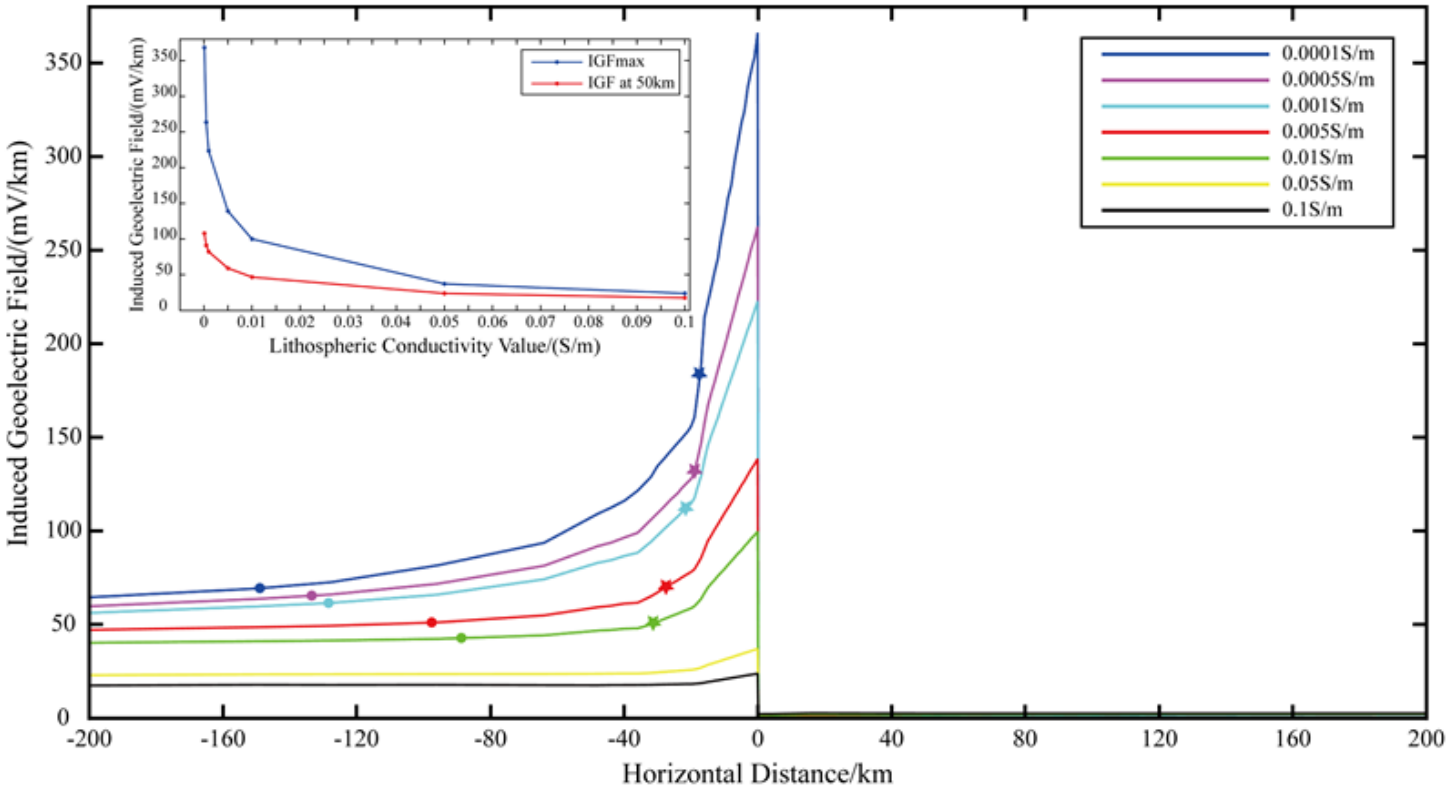

Figure 5

Variation of surface IGF with distance away from the interface for different lithospheric conductivity (0.0001-0.1 S/m). Stars and dots indicate the distance where IGF becomes 50% of IGFmax and IGF nearly stabilizes, respectively, for 0.0001-0.01 S/m. Inset shows the variation of IGFmax (blue) and IGF at 50 km (red) away from the interface with lithospheric conductivity.

Figure 6

(a), (b), (c) and (d), (e), (f) show the distribution of surface IGF and underground IGF, respectively, when the ionospheric current frequency is 0.002 Hz, 0.006 Hz and 0.01 Hz (top to bottom). All other conditions are same as in the model (Figure 2a).

Figure 7

Variation surface IGF with distance away from the interface for different ionospheric current frequency (0.001-0.01HZ). The inset in RHS shows variation of IGFmax (blue) and IGF at 50 km (red) away from the interface with ionospheric current frequency.

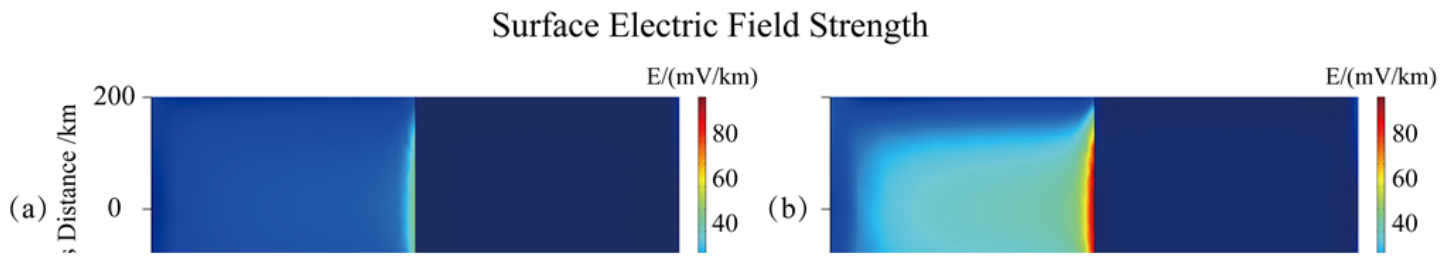

Figure 8

(a), (b) and (c) show the variation of surface IGF (X-Y plane, Z = 0) for current density 50A/m^2, 100A/m^2 and 200A/m^2. (d) is similar to (b) but current density100 A/m^2 is parallel to the interface. All other conditions are same as in the model (Figure 2a).

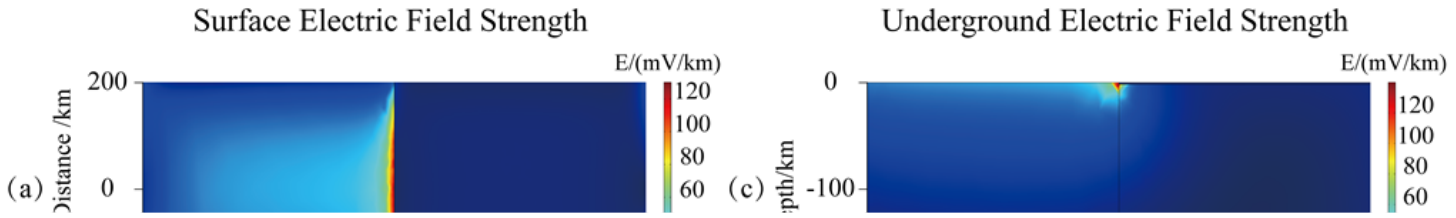

Figure 9

(a), (b) and (c) and (d) show the distribution of surface IGF and underground IGF, respectively, for ocean depth 1 km and 3 km respectively. All other conditions are same as in the model (Figure 2a).

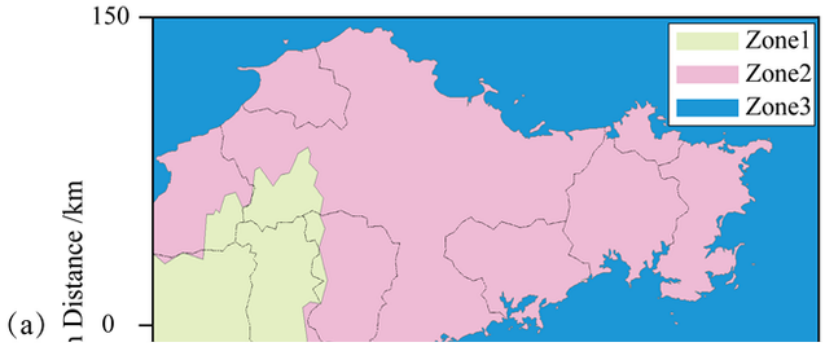

Figure 10

(a) Shows the electrical conductivity map of Jiaodong Peninsula (JDP) of China with list of the 3-D conductivity values. (b) and (c), and (d) and (e) are the distribution of the surface magnetic field and surface IGF simulated for eastward (top) and northward (bottom) ionospheric currents, respectively, in Jiaodong Peninsula (JDP). The results are found to be the same when the current directions are reversed.